EURASIAN PHYSICAL TECHNICAL JOURNAL

2025, Volume 22, No. 3 (53)

https://doi.org/10.31489/2025N3/5-13

Received: 10/04/2025 Revised: 27/05/2025 Accepted: 25/09/2025 Published online: 30/09/2025

Research Article

UDC 539.21; 541.16; 669.784

ANNEALING-INDUCED MORPHOLOGICAL EVOLUTION OF IRON NANOCATALYSTS FOR CARBON NANOTUBE GROWTH

Ismatov A.A.[1*], Romanitan C.[2*], Ashurov Kh.B.[1], Adilov M.M.[1], Rahimov A.A.[1]

[1] Institute of Ion-plasma and laser technologies, Tashkent, Uzbekistan,

[2] National Institute for Research and Development in Microtechnologies, Voluntari, Romania

*Corresponding author: asqarismatov878@gmail.com

Abstract. *The synthesis of iron nanocatalysts on silicon substrates via the Electron Beam Physical Vapor Deposition method has garnered significant attention due to its catalytic uses. The influence of annealing temperature (500°C, 550°C, and 600°C) on the structural and morphological characteristics of Fe nanocatalysts and their use in the growth of carbon nanotubes via Chemical Vapor Deposition is investigated in this study. Atomic Force Microscopy and Scanning Electron Microscopy measurements reveal that an increase in the annealing temperature reduces the average nanocluster size, and annealing at 600°C yields nanoclusters with an average size of approximately 30 nm; hence, they are more effective as catalysts. Raman spectroscopy proved that carbon nanotube growth was only observed on the 600°C-annealed substrate, and it exhibits a high I_D/I_G ratio (<1), indicating high crystallinity and low defect concentration. The absence of Radial Breathing Mode peaks represents additional evidence that the synthesized carbon nanotubes are multi-walled. These findings indicate that nanocluster size and distribution must be controlled with high accuracy using Electron Beam Physical Vapor Deposition and thermal treatment in order to maximize Fe nanocatalysts for carbon nanotubes growth.*

Keywords: Iron nanocatalysts, Carbon nanotube, Physical Vapor Deposition, Chemical Vapor Deposition, Raman spectroscopy, Atomic Force Microscopy, Scanning Electron Microscopy.

1. Introduction

In recent years, metallic nanomaterials have gained widespread popularity due to their physical, chemical, and catalytic properties which make them ideal for use in green chemistry, waste reduction, and environmental remediation [1- 3]. Iron (Fe) nanocatalysts are especially interesting due to the abundancy and low cost of iron, its favorable magnetic characteristics, and versatile reactivity [4,5]. Fe nanocatalysts have numerous applications in chemical synthesis, conversion of renewable energy, and even in cleaning up the environment [6]. Moreover, their involvement in the formation of carbon nanotubes (CNTs) has created a need to refine their synthesis and control their morphology, in order to increase catalytic activity [7] alongside these developments. Central to interest in Fe nanocatalysts is their application in the production of carbon nanotubes. Myriad approaches have been devised for the preparation of Fe nanocatalysts. The most common methods of chemical synthesis include: chemical reduction [8, 9], sol-gel technique [10], thermal evaporation [11], and sputter deposition [12]. Unfortunately, these techniques present important limitation related to the control over the particle size distribution, surface agglomeration, and contamination. It is clear that these features hamper the full potential of the synthesized nanomaterials thus being hampered their

effectiveness [13]. As response to these issues, Electron Beam Physical Vapor Deposition (EB-PVD) has been found to be a highly effective method due to its capacity to function under high vacuum conditions, thereby maintaining low levels of contamination and enabling deposition of very uniform and pure nanostructures [14]. The intrinsic control over deposition parameters of EB-PVD, such as the evaporation rate, substrate temperature or beam current enables the fine adjustment of catalyst morphology, which is a critical factor in optimizing the ensuing catalytic activity and CNT growth [15]. It was demonstrated the possibility to achieve high-purity films and nanostructures by using a ultraclean environment, thus minimizing the formation of defects and contaminants, and the same time promoting fast deposition with less material loss [16]. EB-PVD has also succeeded in optimizing the size and distribution of metallic nanocatalysts, which is essential for high surface area and active site requirements in applications [17]. It has been recently reported that alteration of the annealing conditions following deposition can impose severe changes in the morphology of Fe nanocatalysts, thus further enhancing their catalytic activity for CNT growth [18]. For instance, the reduction in particle size and enhancement in particle uniformity by annealing have been attributed to increased catalytic activity and enhanced crystallinity of CNTs [19]. The current state-of-the-art in CNT synthesis places higher priority on the construction of solid and scalable catalyst preparation methods that can form catalysts of suitable size, distribution, and purity [20]. Despite many physical and chemical methods being tried out, the EB-PVD method is unique in its ability to offer the best balance between controllability and efficiency, especially with the inclusion of subsequent thermal treatments [21]. This mixture not only improves the physical characteristics of the catalyst but also CNT quality and yield in Chemical Vapor Deposition (CVD) conditions [22]. Further, advances in in-situ characterization techniques have also enabled enhanced understanding of nanocatalyst structural evolution on annealing and CNT growth, thus enabling improved process optimization [23]. Despite these advancements, reproducibility of catalyst performance and elucidation of detailed mechanism underlying morphological evolution during the annealing process remains challenging. Numerous works have reported differences in various schemes of annealing and their implications on the character of catalyst, but relationship of deposition parameters with annealing treatment and the resulted synthesis efficiency of CNT remains unclear [24]. Filling this gap is a crucial step for the advancement of the nanocatalyst design field and for the broader application of CNTs in electronics, sensors, and energy storage [25].

In this paper, we report the optimization and synthesis of Fe nanocatalysts via EB-PVD followed by different annealing temperatures (500°C, 550°C, and 600°C). The novelty of our contribution is the rigorous investigation of the annealing-driven morphological evolution and its immediate impact on the growth of CNTs using CVD. With accurate tuning of annealing parameters, we demonstrate a critical temperature for which the nanocatalysts exhibit an ideal size distribution and geometric configuration beneficial for effective nucleation of CNTs. Our experimental outcomes, confirmed with Atomic Force Microscopy (AFM), Scanning Electron Microscopy (SEM), and Raman spectroscopy, reveal that only substrates annealed at 600°C exhibit the properties of the requisite nanoparticles and improved quality CNT growth [26]. This study not only offers a deeper understanding of the inherent mechanisms that control the development of nanocatalysts but also offers a pragmatic route to the synthesis of next-generation catalysts for new applications of CNTs [27].

2. Instrumentals Part

Figure 1 illustrates the setup of an EB-PVD system used for the deposition of Fe nanocatalysts on a silicon substrate. In this configuration, the core components include a vacuum chamber, an electron beam source, and pumping systems to maintain high vacuum conditions essential for precise deposition. The main components and their functions are as follows:

1. Electron Beam Source and Control Panel: The electron beam source is powered by a high-voltage supply, controlled through an interface that allows users to adjust the output voltage in kilovolts (kV). This high-voltage electron beam vaporizes the iron target material, creating a vapor that deposits on the silicon substrate within the vacuum chamber. The control panel includes switches for turning the high voltage (HV) on and off.

2. Vacuum Chamber: The deposition process occurs in the vacuum chamber, which isolates the deposition environment from atmospheric contaminants. Maintaining a high vacuum is crucial for creating uniform nanostructures, as it allows for a controlled deposition process with minimal interference from air particles.

3. Turbomolecular Pump: This pump creates and maintains the high vacuum required for EB-PVD by removing air and other gases from the chamber. It plays a critical role in ensuring that the vaporized material travels directly to the substrate without unwanted reactions or scattering.

4. Asynchronous Rotary Pump: Positioned before the turbomolecular pump, this pump performs initial evacuation, creating a lower vacuum that facilitates the turbomolecular pump's operation. Together, these pumps ensure a clean and stable vacuum environment essential for high-quality nanocatalyst deposition.

5. Cooling Water Lines: Cooling water flows through the system to prevent overheating, which can damage components or alter deposition parameters. This water flow is vital for maintaining temperature stability in both the electron beam source and the pumping system.

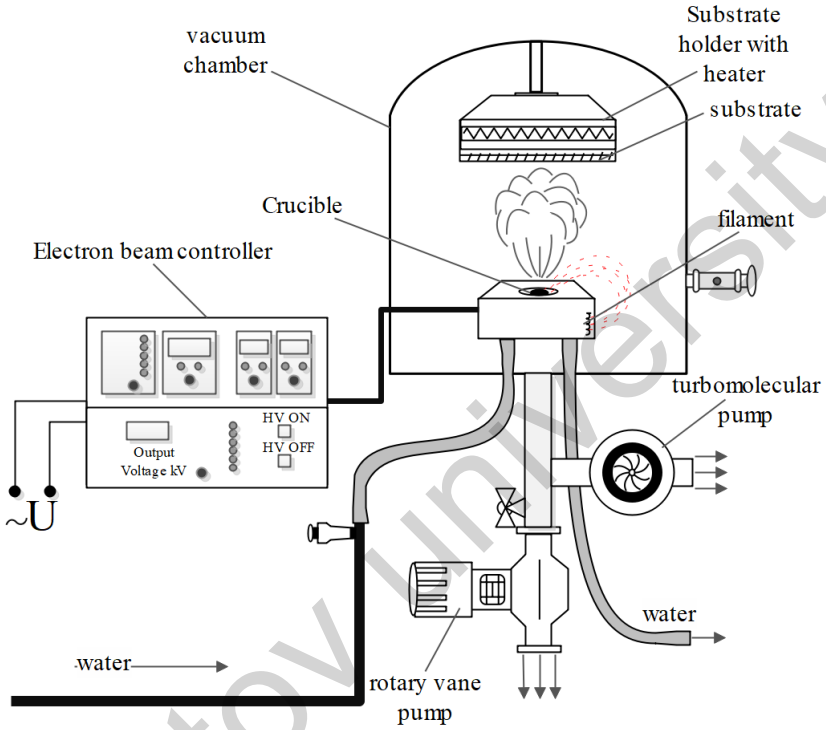

Fig.1. Schematic diagrams` setup of EB-PVD system.

The EB-PVD system operates under high-vacuum conditions, with a chamber pressure of 10^{-6} torr and an applied electron beam voltage of 10 kV, thus providing the precise and stable environment necessary for nanocatalyst deposition. This controlled environment allows a fine-tuning nanocatalyst properties, such as size and morphology, to enhance catalytic performance.

3. Experiment

Silicon wafers (KEC-001, 100, n-type) were sequentially cleaned in three stages, as schematically shown in Figure 2. To form a deposited buffer layer (DBL) on the obtained substrates, an oxide layer was grown using the Thermal Oxidation method. The DBL thickness was controlled by temperature and grown to various thicknesses over a period of 2–5 hours [28]. The substrates were cut into 2 × 1 cm pieces, with two samples taken from each (one directly for CVD after PVD, and the other for analytical characterization).

The prepared substrates were placed in an EB-PVD instrument, where a high-vacuum environment (2–4 × 10^{-6} Torr) was achieved. Iron material, placed in a crucible, was deposited onto the substrate surface for 3 seconds using a cathode filament operated at 10 kV and a current of 30–35 A. During the deposition process, the wafers were maintained at room temperature.

After deposition, under the same vacuum conditions, the iron-coated substrates were annealed at three different temperatures: 500°C, 550°C, and 600°C, each for 30 minutes. Upon completion of the annealing process, the substrates were allowed to cool to room temperature under vacuum before the chamber was opened. A portion of the obtained substrates was immediately transferred to the CVD system.

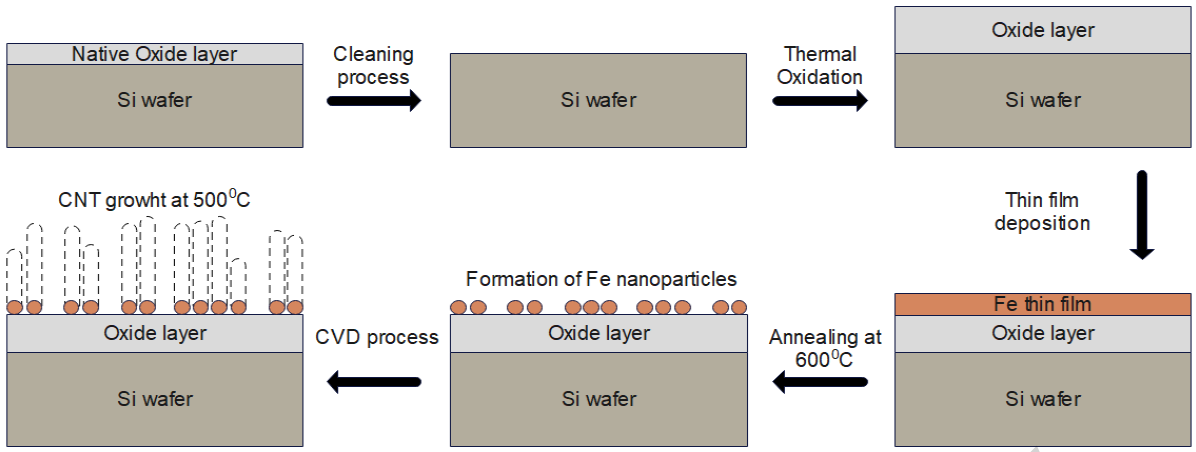

Fig.2. Fe nanocatalyst formation and CNT synthesis via CVD.

The CVD process was also conducted under vacuum conditions. To prevent oxidation of the Fe nanocatalysts' surface, the substrates were reduced in a hydrogen atmosphere at temperatures ranging from 400°C to 500°C for 45 minutes. Subsequently, Ar was introduced as a carrier gas, and an ethanol mixture was supplied as the carbon source into the quartz tube. Regardless of their annealing temperature, both sets of substrates underwent CNT synthesis at 500°C for 1 hour, followed by natural cooling to room temperature.

4. Characterization Techniques

The AFM micrographs were obtained with the equipment NT-MDT Next Solver, operated in semi-contact mode to minimize tip–sample interaction. The scans were performed at a frequency of 1 Hz with a resolution of 300 × 300 pixels, under ambient conditions. This setup enabled precise visualization of the surface morphology and height variations of the catalyst nanoparticles. SEM imaging was conducted using a Thermo Fisher Scientific Apreo 2S LoVac system, operated in low vacuum mode. The system provided a lateral resolution of up to 500 nm, which allowed clear observation of the nanocatalysts' size distribution, surface coverage, and structural uniformity. Raman spectra were acquired using a Renishaw inVia Raman microscope equipped with a 785 nm excitation laser. The measurements were taken in backscattering configuration under ambient conditions. The system offered a spectral resolution better than 1 cm^{-1}, enabling detailed analysis of the D, G, and 2D bands of CNTs to assess their degree of graphitization and structural defects.

5. Results and discussion

Figure 3 presents AFM images on $3 \times 3\ \mu m^2$ of iron nanoclusters annealed at 500°C and 550°C. .One can observe the presence of almost spherical grains distributed on the surface. The size analysis of the nanoclusters revealed that the average diameter of the particles annealed at 500°C was 250 nm (Figure 3a), while those annealed at 550°C exhibited an average diameter of 170 nm (Figure 3b). Only spherical Fe grains can be observed on the surface, without any features on the surface, indicating the absence of CNT growth. This can be attributed to the excessively large size of the nanoclusters, which prevents them from functioning effectively as nanocatalysts. Although carbon atoms adhered to the surface of the nanoclusters, no structured CNT growth was detected.

SEM imaging of iron nanoclusters on substrates annealed at 600°C (Figure 4) demonstrated a significant reduction in particle diameter compared to the samples annealed at the two lower temperatures. The minimum, maximum, and average diameters of the nanoparticles were determined to be 7 nm, 115 nm, and 30 nm, respectively, with a standard deviation (σ) of 15 nm.

This phenomenon indicates that the nanoparticles have reached the critical size required for their functionality as nanocatalysts. Additionally, their geometric shape closely resembles that of droplets (Figure 4a). The particle size distribution derived from SEM analysis indicates that the Fe nanocatalysts have an average diameter of approximately 30 nm. The histogram was constructed using ImageJ software, which

enabled accurate measurement and statistical analysis of nanoparticle dimensions. The distribution shows that the most frequently occurring particle sizes lie within the 15–25 nm range, which is close to the calculated mean. The data exhibits a positively skewed (right-skewed), log-normal distribution, commonly encountered in nanostructure synthesis.

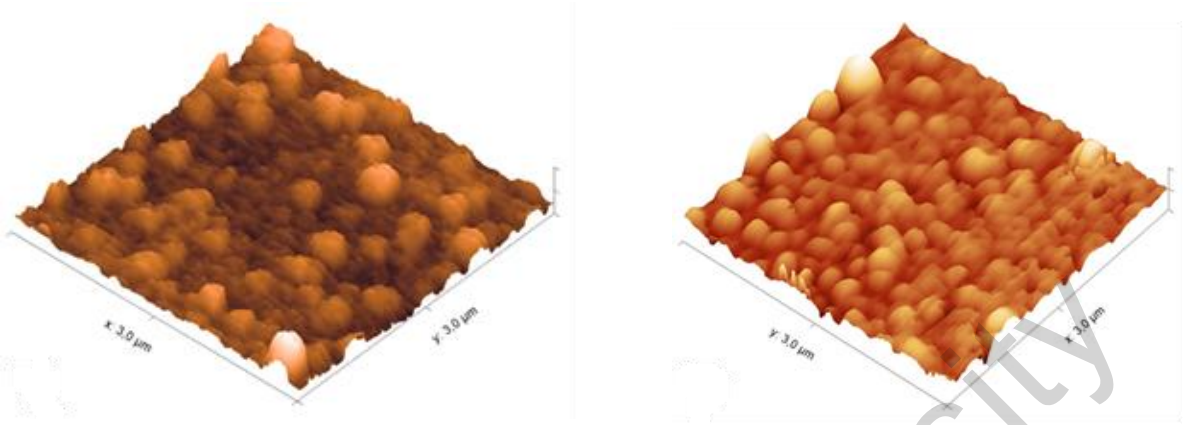

a) b)

Fig.3. AFM images of Fe nanoclusters annealed at 500°C (a) and 550°C (b).

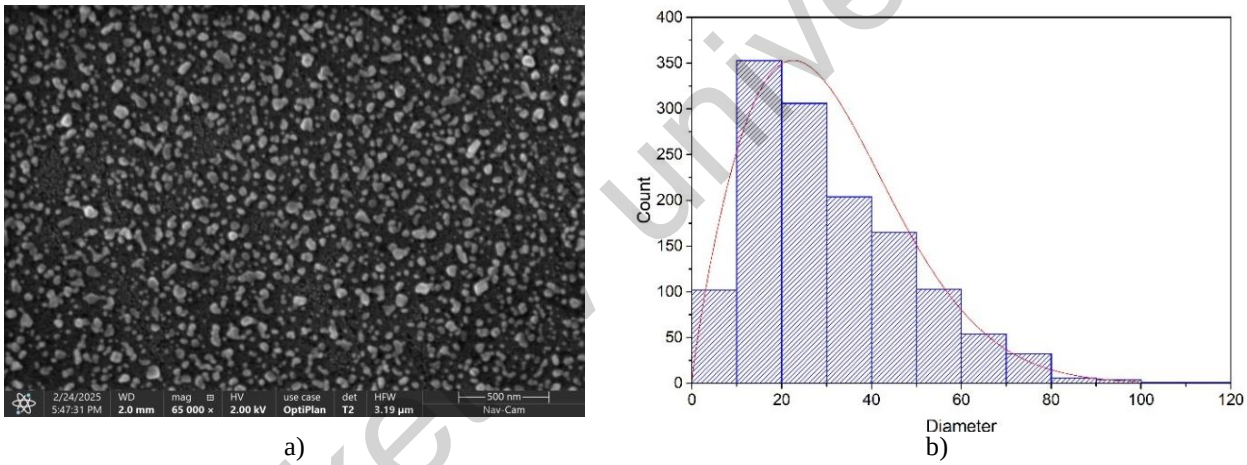

a) b)

Fig.4. (a) SEM image and (b) diameter distribution of Fe nanoparticles annealed at 600°C.

This suggests a high population of small particles, while larger particles are comparatively rare, indicating a polydisperse system. Such non-uniformity in particle size can significantly affect their catalytic behavior during CNT growth (Figure 4b). Furthermore, the appearance of a small number of particles in the 80–100 nm range may be attributed to agglomeration or sintering phenomena occurring during deposition or annealing processes. This confirms that 600°C represents the threshold temperature at which the iron thin film transforms into catalytically active nanoparticles.

EDX analysis further confirmed that the elemental composition of the substrate is uniformly distributed across the surface, as depicted in Figure 5a, b, and c. The absence of foreign elements in the sample serves as evidence of the high precision and purity maintained during the nanocatalyst preparation process.

Additionally, Figure 5d illustrates the percentage composition of the elements, providing insight into their relative abundance within the overall sample.

Raman spectroscopy (785 nm laser) analysis conducted after the CVD process confirmed that no CNT growth occurred on the surfaces of the substrates annealed at 500°C and 550°C. However, CNT formation was observed on the 600°C-annealed substrate after CVD at 500°C (Figure 6).

The Raman spectrum displayed a dominant G band at 1582 cm^{-1} compared to the D band at 1326 cm^{-1}. The intensity ratio of D to G (I_D/I_G) corresponded to 0,56 , indicating high crystallinity and low defectiveness in the CNTs. Compared to the MWCNTs grown in [29], the obtained results indicate significantly higher quality. According to the best Raman analysis results of MWCNTs synthesized by Miura

et al., the I_D/I_G ratio was found to be 1,11. Our results suggest an approximately twofold improvement in I_D/I_G over them, a finding that complements rather than contradicts their contributions. The smaller this ratio, the more ordered and high-quality the nanotubes are. If the intensity ratio of the D peak to the G peak is less than 0,5, it indicates highly ordered and high-quality nanotubes.

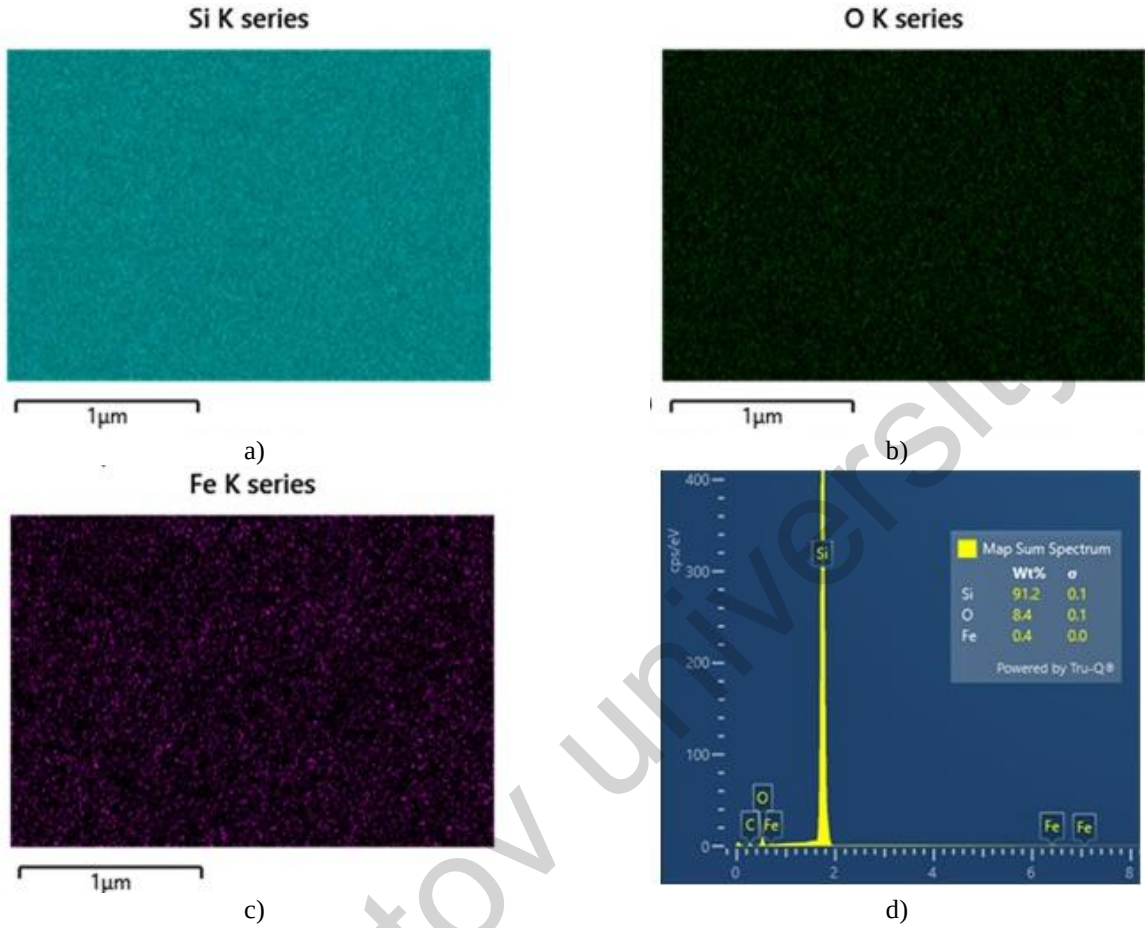

Fig.5. EDX analysis of nanoparticles annealed at 600°C: (a), (b), (c), and (d).

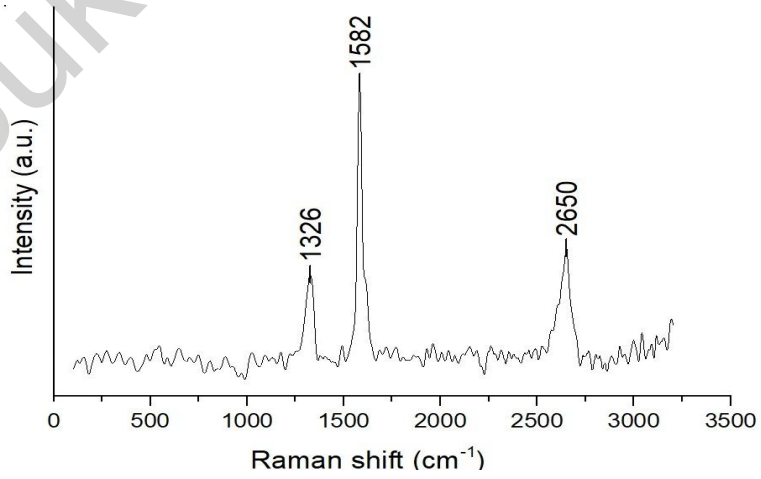

Fig.6. Raman spectrum of CNTs grown on Fe nanoparticles annealing at 600 ^{0}C.

If this ratio falls within the range of 0,5 to 1, it suggests the presence of some defects; however, the nanotubes remain structurally viable. Furthermore, the absence of RBM peaks in the 100–400 cm^{-1} range confirmed that the synthesized CNTs were multi-walled rather than single-walled.

6. Conclusion

In the present study, Fe nanocatalysts were successfully grown on Si substrates by means of Electron Beam Physical Vapor Deposition (EB-PVD) and subsequently subjected to annealing at various temperatures (500, 550, and 600 °C). The variation of annealing temperature was investigated for optimizing the structural and morphological characteristics of Fe nanoclusters to be used as catalysts in the growth of carbon nanotubes (CNTs). From Atomic Force Microscopy (AFM) and Scanning Electron Microscopy (SEM) investigations, it is confirmed that the higher annealing temperature attributed to the decrease in nanocluster size, with the most favorable size distribution at 600° ranging from 7–115 nm (average 30 nm). Raman spectra show CNTs only after annealing at 600°C with an ID/IG of 0.56, a value associated with high crystallinity and low defect levels. Taken together with prior studies under the same conditions, these data point to an approximate twofold reduction in ID/IG, implying enhanced structural quality. Based on the SEM-derived size distribution of the nanoparticles, the samples are consistent with multi-walled carbon nanotubes. In addition, the absence of Radial Breathing Mode peaks further elaborated this conclusion.

The iron nanocatalysts obtained in this study have great potential for various advanced fields such as nanoelectronics, nanomedicine, energy storage and conversion, environmental remediation, and sensor technologies, where precise control over nanoparticle size is crucial for optimizing performance; therefore, the method developed here, which enables fine-tuning of nanocluster dimensions, represents a highly valuable approach that not only advances these fields but also provides evidence that controlling the nanocatalyst size and distribution can optimize their use in carbon nanotube synthesis, with the EB-PVD technique under appropriate annealing conditions offering an effective way to produce high-quality nanocatalysts possessing uniform morphology and enhanced catalytic efficiency, while further refinement of deposition and annealing parameters is expected to enable even more precise control over nanostructure formation and catalytic performance, and in addition, exploring other catalyst materials and substrate modifications may open new avenues for improving processes related to CNT synthesis.

Conflict of interest statement

The authors declare that they have no conflict of interest in relation to this research, whether financial, personal, authorship or otherwise, that could affect the research and its results presented in this paper.

CRediT author statement

A.A. Ismatov: Writing – original draft, Investigation, Formal analysis, Visualization, **C. Romanitan**: Methodology, Formal analysis, Writing – review & editing, **Kh. B. Ashurov**: Supervision, Funding acquisition, **M.M. Adilov**: Conceptualization, Methodology, **A.A. Rahimov**: Investigation. The final manuscript was read and approved by all authors.

Funding

The authors gratefully acknowledge the financial and technical support provided by the Ministry of Higher Education, Science and Innovation under project number IL-5421101842

Acknowledgements

I would like to thank the team of the Institute of Ion-Plasma and Laser Technologies, Center for Collective Use of Scientific Instruments

References

1 Vaz C.A.F., Piamonteze C., Kleibert A. (2018) Enhanced mobility of iron nanoparticles deposited onto a xenon-buffered silicon substrate. *Journal of Magnetism and Magnetic Materials*, *459*, 2-6. https://doi.org/10.1016/J.JMMM.2018.02.021

2 Melchionna M., Fornasiero P., Cargnello M. (2017) Opportunities and Challenges in the Synthesis, Characterization, and Catalytic Properties of Controlled Nanostructures. *Studies in Surface Science and Catalysis*,177, 1-56. https://doi.org/10.1016/B978-0-12-805090-3.00001-2

3 Movchan B. A. (2016) Discrete nanosized metallic coatings produced by EB-PVD. *Surface Engineering*, 32, 4. https://doi.org/10.1179/1743294415Y.0000000092

4 Lehmann H.W., Frick K. (1988) Optimizing deposition parameters of electron beam evaporated TiO_2 films. *Applied Optics*, 27, 4920-4924**.** https://doi.org/10.1364/AO.27.004920

5 Minea T.M., Point S., Gohier A., Granier A., Godon C., Alvarez F. (2005) Single chamber PVD/PECVD process for in situ control of the catalyst activity on carbon nanotubes growth. *Surface and Coatings Technology*, *200*(1-4), 1101-1105. https://doi.org/10.1016/J.SURFCOAT.2005.01.053

6 Sharapov I., Omarova G., Sadykova A., Seliverstova E. (2025) Properties of Ag/TiO_2 AND Ag/SiO_2 nanoparticles and their effect on the photocatalytic properties of a semiconductor nanocomposite. *Eurasian Physical Technical Journal*, *22*(2 (52)), 25–32. https://doi.org/10.31489/2025N2/25-32

7 Berdiev U., Khudaykulov I., Iskandarov S., Amirova A., Ashurov K. (2025) Influence of SiO2 Nanoparticles on the Characteristics of a Polyvinyl Alcohol-Based Proton Exchange Composite Membrane. *East European Journal of Physics*, (1), 265-271. https://doi.org/10.26565/2312-4334-2025-1-30

8 Melchionna M., Beltram A., Stopin A., Montini T., Lodge R. W., Khlobystov A.N., . Fornasiero P. (2018) Magnetic shepherding of nanocatalysts through hierarchically-assembled Fe-filled CNTs hybrids. *Applied Catalysis B: Environmental*, 227, 356-365. https://doi.org/10.1016/j.apcatb.2018.01.049

9 Sharma P., Pavelyev V., Kumar S., Mishra P., Islam S.S., Tripathi N. (2020) Analysis on the synthesis of vertically aligned carbon nanotubes: growth mechanism and techniques. *Journal of Materials Science: Materials in Electronics*, *31*(6), 4399-4443. Available at: https://link.springer.com/article/10.1007/s10854-020-03021-6

10 Ju L., Chen Z., Fang L., Dong W., Zheng F., Shen M. (2011) Sol–gel synthesis and photo- Fenton- like catalytic activity of EuFeO3 nanoparticles. *Journal of the American Ceramic Society*, 94(10), 3418-3424. https://doi.org/10.1111/j.1551-2916.2011.04522.x

11 Dai Z.R., Pan Z.W., Wang Z.L. (2003) Novel nanostructures of functional oxides synthesized by thermal evaporation. *Advanced Functional Materials*, 13(1), 9-24. https://doi.org/10.1002/adfm.200390013

12 Bosso P., Del Sole R., Milella A., Mengucci P., Barucca G., Armenise V., & Palumbo F. (2023) Nanostructured iron oxide thin films deposited by RF sputtering as catalysts for the heterogeneous solar photo-Fenton reaction. *Vacuum*, *207*, 111646. https://doi.org/10.1016/j.vacuum.2022.111646

13 Zeng Xiaoliang, Yu Shuhui, Ye Lei, Li Mingyan, Pan Zhilong, Sun Rong, Xu J.B.. (2014) Encapsulating carbon nanotubes with SiO2: A strategy for applying them in polymer nanocomposites with high mechanical strength and electrical insulation. *J. Mater. Chem. C.*, 3, 187-195. http://dx.doi.org/10.1039/C4TC01051E

14 Zhang Q., Cheng G., Zheng R. (2018) The Internal Buckling Behavior Induced by Growth Self-restriction in Vertical Multi-walled Carbon Nanotube Arrays. *MRS Advances*, *3*(45–46), 2815–2823. https://doi.org/10.1557/adv.2018.429

15 Jing L., Li H., Lin J., Tay R.Y., Tsang S.H., Teo E.H.T., Tok A.I.Y. (2018) Supercompressible coaxial carbon nanotube@ graphene arrays with invariant viscoelasticity over− 100 to 500 C in ambient air. *ACS Applied Materials & Interfaces*, *10*(11), 9688-9695. Available at: https://pubs.acs.org/doi/abs/10.1021/acsami.8b01925

16 Eres G., Rouleau C. M., Puretzky A. A., Geohegan D.B., Wang H. (2018) Cooperative behavior in the evolution of alignment and structure in vertically aligned carbon-nanotube arrays grown using chemical vapor deposition. *Physical Review Applied*, *10*(2), 024010. https://doi.org/10.1103/PhysRevApplied.10.024010

17 Walsh P.J., Li H., Anaya de Parrodi C. (2007) A green chemistry approach to asymmetric catalysis: Solvent-free and highly concentrated reactions. *ChemInform*, 38(30), 112–118. https://doi.org/10.1002/chin.200736264

18 Păun C., Obreja C., Comănescu F., Tucureanu V., Tutunaru O., Romaniţan C., Ionescu O. (2019). Epoxy nanocomposites based on MWCNT. *Proceeding of the IEEE 2019 International Semiconductor Conference (CAS)*, 237 – 240. https://doi.org/10.1109/SMICND.2019.8923947

19 Paun C., Obreja C., Comanescu F., Tucureanu V., Tutunaru O., Romanitan C., & Paltanea G. (2021) Studies on structural MWCNT/epoxy nanocomposites for EMI shielding applications. *Proceeding of the IOP Conference Series: Materials Science and Engineering*, 1009, 1, 012046. https://doi.org/10.1088/1757-899X/1009/1/012046

20 Hu H., Xin J.H., Hu H., Wang X., Miao D., Liu Y. (2015) Synthesis and stabilization of metal nanocatalysts for reduction reactions–a review. *Journal of materials chemistry A*, 3(21), 11157-11182. https://doi.org/10.1039/C5TA00753D

21 Rusevova K., Kopinke F.D., Georgi A. (2012) Nano-sized magnetic iron oxides as catalysts for heterogeneous Fenton-like reactions—Influence of Fe (II)/Fe (III) ratio on catalytic performance. *Journal of hazardous materials*, 241, 433-440. https://doi.org/10.1016/j.jhazmat.2012.09.068

22 Abdisaidov I., Khudaykulov Ilyos, Ashurov Kh. (2024) Low-temperature growth of carbon nanotubes using nickel catalyst. *East European Journal of Physics*., 355-358. https://doi.org/10.26565/2312-4334-2024-3-41

23 Mohapatra M., Anand S. (2010) Synthesis and applications of nano-structured iron oxides/hydroxides–a review. *International Journal of Engineering, Science and Technology*, 2(8). https://doi.org/10.4314/ijest.v2i8.63846

24 Ali A., Zafar H., Zia M., ul Haq I., Phull A.R., Ali J. S., Hussain A. (2016) Synthesis, characterization, applications, and challenges of iron oxide nanoparticles. *Nanotechnology, science and applications*, 49-67. https://doi.org/10.2147/NSA.S99986

25 Khan Y., Sadia H., Ali Shah S.Z., Khan M.N., Shah A.A., Ullah N., Khan M.I. (2022) Classification, synthetic, and characterization approaches to nanoparticles, and their applications in various fields of nanotechnology: a review. *Catalysts*, 12(11), 1386. https://doi.org/10.3390/catal12111386

26 Campos E. A., Pinto D.V.B.S., Oliveira J. I. S. D., Mattos E.D.C., Dutra R.D.C.L. (2015) Synthesis, characterization and applications of iron oxide nanoparticles-a short review. *Journal of Aerospace Technology and Management*, 7(3), 267-276. https://doi.org/10.5028/jatm.v7i3.471

27 Karakashov B., Mayne-L'Hermite M., Pinault M. (2022) Conducting interface for efficient growth of vertically aligned carbon nanotubes: Towards nano-engineered carbon composite. *Nanomaterials*, 12(13), 2300. https://doi.org/10.3390/nano12132300

28 Ashurov X., Adilov M., Ismatov A., Rakhimov A. (2025) Oxide layer growth on silicon substrates: effects of temperature and surface preparation. *Uzbek Journal of Physics*, 26(4). https://doi.org/10.52304/.v26i4.570

29 Miura S., Yoshihara Y., Asaka M., Hasegawa K., Sugime H., Ota A., Oshima H., Noda S. (2018) Millimeter-tall carbon nanotube arrays grown on aluminum substrates. *Carbon*, *130*, 834-842. https://doi.org/10.1016/j.carbon.2018.01.075

AUTHORS' INFORMATION

Ismatov, Askar Anvar o`g`li – Master (Sci.), Scientific Researcher, Institute of ion plasma and laser technologies, Tashkent, Uzbekistan; https://orcid.org/0009-0006-5005-4201; asqarismatov878@gmail.com

Romanitan, Cosmin - PhD, Physics Research Scientist, Voluntari, National Institute for Research and Development in Microtechnologies, Bucharest, Romania; Scopus Author ID: 56829395900, https://orcid.org/0000-0002-5615-6624; cosmin.romanitan@imt.ro

Adilov, Mukhammadjon Masharipovich - PhD, Head of the laboratory, Institute of ion plasma and laser technologies, Tashkent, Uzbekistan; Scopus Author ID: 55291303400, https://orcid.org/0000-0003-0312-2356, muhammad.84@mail.ru

Rakhimov, Abdulla Abdumurod o`g`li – Master (Sci.), Scientific Researcher, Durman street 33, Institute of ion plasma and laser technologies, Tashkent, Uzbekistan; https://orcid.org/0009-0004-1687-0454 , abdullarakhimov55@gmail.com

Ashurov, Khatam Baxronovich – D.Sc., Professor, Institute of ion plasma and laser technologies, Tashkent, Uzbekistan; Scopus Author ID: 23391831300, https://orcid.org/0000-0002-7604-2333; ashurov@iplt.uz